The Behavior of Fixed Point Iteration and Newton-Raphson Methods in Solving the Blade Element Momentum Equations

Michael McWilliam[1] and Curran Crawford[2]
[1]*PhD Candidate, mmcwilli@uvic.ca*
[2]*Assistant Professor, curranc@uvic.ca*
Sustainable Systems Design Laboratory, Department of Mechanical Engineering, University of Victoria, 3800 Finnerty Road, Victoria, British Columbia, Canada
December 16, 2010

ABSTRACT
There is a substantial body of ongoing research improving the Blade Element Momentum (BEM) theory and applying it to the optimization of wind turbine rotors. Both of these developments challenge the suitability of fixed point iteration schemes being applied to advanced BEM models. This article explores the mathematical behavior of the BEM equations, with special attention to the application of numerical methods. Under special conditions, multiple solutions will exist when the airfoil is stalled. This situation gives increased uncertainty, where uncertainty in airfoil behavior is already high. This also demonstrates that there could be circumstances where the wake state has weak dependence on blade state. Fixed point iteration and Newton-Raphson numerical methods are investigated in this paper. Both methods will become unstable under certain conditions. The investigation shows that the Newton-Raphson method has well defined conditions for instability in terms of design variables and airfoil properties. By comparison, the fixed point function used here exhibits instability over a larger range.

1. INTRODUCTION
Blade Element Momentum (BEM) theory is widely used to model the aerodynamic performance of wind turbines. The efficiency of these methods has made them common in many design codes. Despite their inherent simplicity, these methods have proven reliable enough for design and certification. Consequently, there is still active research into design methods based on BEM theory [1].

Despite their widespread use, these methods have several shortcomings. Owing to the basic assumptions, they are not suitable for out-of plane blade geometry, like coning and winglets. Furthermore, the assumption of radial independence between the sections undermines their validity in unsteady flows. Thus, the methods are limited for modeling yawed flow and highly stalled conditions, often seen in turbine operation. Several models have been proposed in recent history to deal with these issues.

The work of Du and Tangler has addressed the problem of stall delay [2, 3]. Shen has provided alternative models for the tip loss effects [4]. Other researchers have focused more on problems regarding the momentum model. Chaney *et al.* developed a method for incorporating the effects of an expanding wake [5]. Madsen *et al.* compared BEM to actuator

disc models to develop two correction models for deviations in the local power coefficients [6]. Haans *et al.* developed an advanced model for yawed flow [7]. The work of Crawford gave a novel way of modeling coned rotors [8]. Finally, Sharpe incorporated wake rotation effects play in the axial momentum equations [9, 10]. Martinez *et al.* has used the momentum model developed by Sharpe, along with airfoil post stall corrections, to give improved predictions for stall regulated wind turbines [11].

Due to its efficiency, BEM theory is being applied in turbine optimization tools. Xudong *et al.* have successfully applied BEM based optimization to design several wind turbines of various sizes [12]. The early work of Fuglsang *et al.* created a Multi-Disciplinary Optimization framework with BEM, structural and fatigue models to minimize the cost of electricity, with sequential linear programming and the method of feasible directions [13]. The work of Clifton-Smith et. al. applied genetic algorithms with BEM to optimize energy capture and startup time [14, 15]. The work of Benini *et al.* is another example of applying genetic algorithms, in this case applied to the multi-objective optimization of a stall regulated wind turbine [16]. The work of Crawford *et al.* applied BEM with a generator model and a low frequency noise model to optimize the turbine for minimal cost of electricity and minimum energy pay back period, with gradient based techniques [17]. Another work by Crawford *et al.* applied gradient based techniques with advanced BEM methods to optimize a unique rotor design that had hinged rotor blades [18]. The importance of convergence is touched upon by Lanzafame, who demonstrated why sources of numerical instability must be reduced in optimization applications [19]. Similarly, the work of Hjort *et al.* showed how poor convergence introduces noise into the optimization. This noise compromised the gradient calculations, thus, undermining any gradient based methods in their study [20].

The typical approach to solving the momentum equations is to analytically reformulate the expression as a fixed point function. Here, the induction at a future iteration is expressed as a function of induction at the current iteration. For the basic BEM equations, this method is both fast and accurate. However, the benefits of a fixed point scheme are diminished in many of these advanced BEM models. The work by Crawford showed that applying the out-of-plane correction models in unsteady simulations slowed the convergence [21]. Furthermore, the implicit definition of induction in the momentum equations given by Sharpe makes it difficult to formulate a fixed point iteration function [9]. Thus, the fixed point iteration scheme may not be suitable as a general solver for all forms of BEM. It is clear that other numerical techniques need to be investigated to enable the use of all advanced BEM based methods.

When a method is applied in a optimization application, the numerical method must be both stable and efficient for it to be practical [19, 20]. This defines the criteria for evaluating an alternative method. The Newton-Raphson technique has very fast convergence, however it also comes with known instabilities. Fortunately, these instabilities can be detected and dealt with by other methods. Overall, this article investigates numerical methods for solving the BEM equations. This paper first explores analytically the predicted behavior of the BEM equations. The stability of two numerical methods is then quantified over a range of parameters, followed by recommendations for the application of these methods. Speed is not the focus of this article; the numerical methods under consideration are fast for most problems, thus we assume that each method already meets the efficiency criteria.

The approach taken in this article explores a basic form of the BEM equations. This allows the major trends of the equations to be identified quickly and simply. The equations selected here will have a similar form to the more advanced forms that motivated this work. This similarity will make the conclusions drawn here applicable to other forms of BEM. Many of the conclusions from this study will apply to any monotonic momentum equation. The

conservation of momentum requires any such model to be monotonic, hence, these conclusions are universal. Furthermore, only the axial momentum equation is explored, with a simple turbulent wake correction model. Neglecting the tangential component of BEM theory is justified since it has a small influence of the final solution.

2. BLADE ELEMENT MOMENTUM THEORY

The key parameter in solving the momentum equations is the induction at the rotor plane. This affects the angle of attack and all the aerodynamic forces on the blade. The induction solution is achieved when the thrust coefficient of the axial momentum equation (1) equals the thrust coefficient of the blade element equation (2).

$$C_{tm} = 4a\,(1 - a) \tag{1}$$

$$C_{tb} = \sigma \left(\frac{W}{V_\infty} \right)^2 c_n \tag{2}$$

Both equations give the coefficient of thrust C_t, which is a non-dimensional thrust parameter. The induction is given by a; its effect on equation (2) is not obvious, but will be shown in the definition of the terms in equation (2). The effect of blade size is captured in the solidity term (σ); this is the ratio of blade area to swept area. The effect of the airfoils is captured by the normal force coefficient; this parameter is found with equation (3). Here, the sectional coefficient of lift (c_l) and sectional coefficient of drag (c_d) are dependent on the angle of attack (α), which is the difference between the local flow angle (ϕ) and the twist angle (θ) - see equation (4) and figure 1. The local flow angle is governed by equation (5), where λ is the local speed ratio, which is the ratio of the blade speed to the undisturbed wind

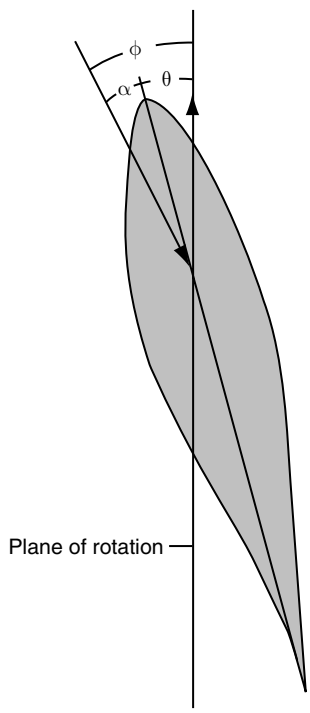

Figure 1: Geometric convention for blade element theory.

velocity. The effect of the rotor's angular speed is captured by the velocity ratio (W/V_∞); this is the ratio of air speed relative to the blade, to the undisturbed wind speed. This parameter can be given in terms of model variables with either expression (6) or (7). For the remainder of the discussion, only the first version (6) will be considered.

$$c_n = c_l \cos\phi + c_d \sin\phi \tag{3}$$

$$\alpha = \phi - \theta \tag{4}$$

$$\tan\phi = \frac{1-a}{\lambda} \tag{5}$$

$$\frac{W}{V_\infty} = \frac{1-a}{\sin\phi} \tag{6}$$

$$\frac{W}{V_\infty} = \frac{\lambda}{\cos\phi} \tag{7}$$

The domain of the axial momentum equation (1) is limited to low values of thrust before a turbulent wake state is entered. When circumstances arise where the thrust is too high, the turbulent wake function is used instead, equation (8). The function given here is not strictly based on experimental data or models presented in literature, but selected for its simplicity to illustrate the numerics of the methods. The analytic study will not look at the turbulent wake state, leaving its examination to the numerical study in section 3.

$$C_{tw} = \frac{5.2a + 0.8}{3} \tag{8}$$

2.1. Application of a Newton-Raphson Iteration Scheme

The residual expression, equation (9), is given by subtracting equation (2) from equation (1). This equation is used by a Newton-Raphson iteration algorithm to find a solution for a. Numerical instabilities will occur when the slope of this equation approaches 0. The circumstances for this condition to occur can be investigated by differentiating equation (9), to yield equation (10).

$$R(a) = 4a(1-a) - \sigma\left(\frac{1-a}{\sin\phi}\right)^2 c_n \tag{9}$$

$$\frac{dR}{da} = \overbrace{4-8a}^{I} + \sigma\overbrace{\left(\underbrace{2(1-a)c_n}_{A} + \lambda\underbrace{\left(\overbrace{\frac{dc_l}{d\alpha}\cos\phi}^{i} + \overbrace{\frac{dc_d}{d\alpha}\sin\phi}^{ii} + \overbrace{c_d\cos\phi}^{iii} - \overbrace{c_l\sin\phi}^{iv}\right)}_{B}\right)}^{II} \tag{10}$$

Term I in equation (10) is the gradient of the momentum equation; this term is always positive for any realistic model, including turbulent wake models. The source of the instability is the blade element gradient, labeled as term II. An important quality is that solidity acts as

an amplifier for this term, thus any negative quantity for the right hand side of II can yield an instability if solidity is scaled properly.

Further insight can be gained by looking where terms A and B combine to give a negative quantity. Term A accounts for the effect of changing W/V_∞. The first component of this term will only be negative when the turbine is reversing the flow. The second component has similar trends, and will only be negative when the blade element is applying forces that accelerate the flow. Thus, this term can only contribute to instability when the rotor is operating in off-design conditions. For a well designed turbine, this instability is rare.

The B term accounts for variation in the blade force term. The first variable in this term is the local speed ratio; like solidity, this term can be considered an amplifier. The remaining terms are dependent on the blade element state. Here the angle of attack has a strong influence. This would give strong coupling to the blade twist and local speed ratio. The first two terms account for the change in lift and drag coefficients. The remaining terms account for variation in the direction of blade forces.

The first term (i) shows that a negative lift slope can lead to instability; this will occur when the blade is stalling at either positive or negative angles of attack. The second term (ii) shows that variation in drag contributes to stability at positive angles of attack, and is detrimental elsewhere. The third term (iii) shows that the actual drag force has a stabilizing effect overall. The fourth term (iv) shows that the lift force can have a stabilizing effect at negative angles of attack, but introduce instability as the flow angle increases, and lift forces are high.

2.2. Application to Fixed Point Iteration Scheme

The fixed point iteration function for the BEM equations is developed by assuming that the flow angle is constant, then solving equations (9) for $R(a) = 0$. The fixed point iteration function for the version of BEM presented here is given in equation (11).

$$a_{i+1} = f(a) = \frac{1}{\frac{4\sin^2\phi}{\sigma c_n} + 1} \tag{11}$$

By explicitly defining induction as a function of blade conditions, the only source of instability is in the lift and drag response of the blade itself. A fixed point iteration will diverge, whenever the gradient of the function $f(a)$ has a magnitude of 1 or greater. This condition was applied to equation (11), to define the conditions for stability given by equation (12). The reader should be aware that both equation (11) and (12), are not valid beyond the onset of turbulent wake conditions.

$$\begin{cases} \dfrac{dc_n}{d\phi} > \overbrace{\cos\phi c_n}^{I} - \overbrace{\left(\dfrac{\lambda^2 + (1-a)^2}{\lambda}\right)\dfrac{(4\sin^2\phi + \sigma c_n)^2}{4\sigma\sin^2\phi}}^{II} & \text{for } \sin^2\phi\dfrac{dc_n}{d\phi} > \sin(2\phi)c_n \\ 0 < (4\sin^2\phi + \sigma c_n)^2 & \text{for } \sin^2\phi\dfrac{dc_n}{d\phi} = \sin(2\phi)c_n \\ \dfrac{dc_n}{d\phi} < \cos\phi c_n + \left(\dfrac{\lambda^2 + (1-a)^2}{\lambda}\right)\dfrac{(4\sin^2\phi + \sigma c_n)^2}{4\sigma\sin^2\phi} & \text{for } \sin^2\phi\dfrac{dc_n}{d\phi} < \sin(2\phi)c_n \end{cases} \tag{12}$$

The inequality given in equation (12) shows three conditions. Which equation is active is dependent on a domain constraint. The middle condition can be ignored, as this will only be

active when the turbulent wake conditions occur and this expression is not valid in any case. The left hand side of all the inequalities is dependent on the variation of the normal force coefficient. Note that $\frac{dc_n}{d\phi}$ is related to airfoil coefficients through equation (13). The right hand side of all the conditions is a function of the normal force coefficient. Inspection of equation (12) shows that the stability condition is similar to the domain constraint. This means that it is likely that the favorable condition will be active, giving a bias towards stability.

$$\frac{dc_n}{d\phi} = \frac{dc_l}{d\alpha}\cos\phi + \frac{dc_d}{d\alpha}\sin\phi + c_d\cos\phi - c_l\sin\phi \tag{13}$$

Stability cannot be guaranteed however, since the first condition can be active whenever the normal force gradient is relatively large. Under these conditions, divergence occurs when the normal force coefficient is still large enough that term II is similar in magnitude to term I. This may occur over a wide range of flow angles.

Another source of instability is in the turbulent wake functions. Each turbulent wake model can form a residual expression that could be solved to develop a fixed point function. For the turbulent wake model used here, the fixed point function resembled the quadratic formula. For the equation used in this study, the domain is bounded, and the range is unbounded. Both of these qualities would lead to a diverging solution. Other turbulent wake models would have a different form, with their own unique stability characteristics.

An important point to note is that in a Newton-Raphson iteration, the stability is independent of the momentum model, and strongly dependent on the airfoil characteristics. The stability characteristics of a fixed point scheme are far more complicated, and unique for every momentum model or turbulent wake model.

3. NUMERICAL ANALYSIS

To expand on the analytic investigation, a set of numerical results were analyzed. The first goal was to identify a) whether multiple solutions to the BEM equations could exist, then b) regions of numerical instability and finally c) how well these regions correlated with the angle of attack. The role of airfoil drag is debatable. Some researchers propose that it should not be used to determine the induction, since the effect of drag in the momentum balance is limited to a narrow region of the wake [22]. Other researchers assume an azimuthal averaged loss of momentum, that includes the effect of drag [21]. To explore the effect of these assumptions, a second set of data was generated, without using the drag coefficient.

3.1. Details of the Study

The theory described in section 2 was implemented in a computer program. The theory has four independent variables: blade twist (θ), the local speed ratio (λ), solidity (σ) and axial induction (a). The first three are effectively design parameters fixed by section location, rotor speed and inflow conditions, while the last one is a state variable that would be iterated on by a numerical solver.

For a given set of design parameters, the code sampled induction values 'a' between -0.25 and 1.0 inclusive with a step size of 0.001. From that, the code determined the values of equation (9) and equation (11) at each point. To evaluate stability, finite differencing was applied to obtain the slope of each equation. Locations where the sign of the residual expression changed were counted as a solution to the BEM equation. These calculations were then applied over a large range of design parameters.

The code used the lift and drag data from eight S800 series airfoils (S801, S809, S810, S812, S813, S814, S815 and S825). The airfoils were chosen for the availability of experimental data over a wide range of angle of attack [23, 24, 25, 26, 27, 28, 29, 30]. A second set of data for a rough leading edge was also used for each airfoil. To prevent angle of attack domain errors, the airfoil data was extrapolated to ±180° using methods proposed by the National Renewable Energy Laboratory (NREL) [31]. This extrapolation is common practice in turbine design. Linear interpolation was applied for intermediate α points.

3.2. The Existence of Multiple Solutions

For every airfoil both clean and rough, regardless of whether drag was used or not, there were regions within the design space where multiple induction solutions existed. Most had 3 unique solutions, but some points had up to 5. The regions where multiple solutions exist is given by figure 2. Each contour plot is defined by two design variables, while the value is defined by the maximum number of solutions for all the points of the remaining design variable. Figures 2a through 2c are typical for most airfoils in the study. Here, the results show that the region of multiple solutions is nearly planar within the 3-dimensional space defined by the design parameters. In this region the design parameters allow the blade element model to follow the momentum model. The BEM equations with the clean S812, rough S814 and rough S815 have multiple solutions over a much wider range of the design space. An example of this is given by figure 2d. Thus, no assumptions can be made on where multiple solutions will exist.

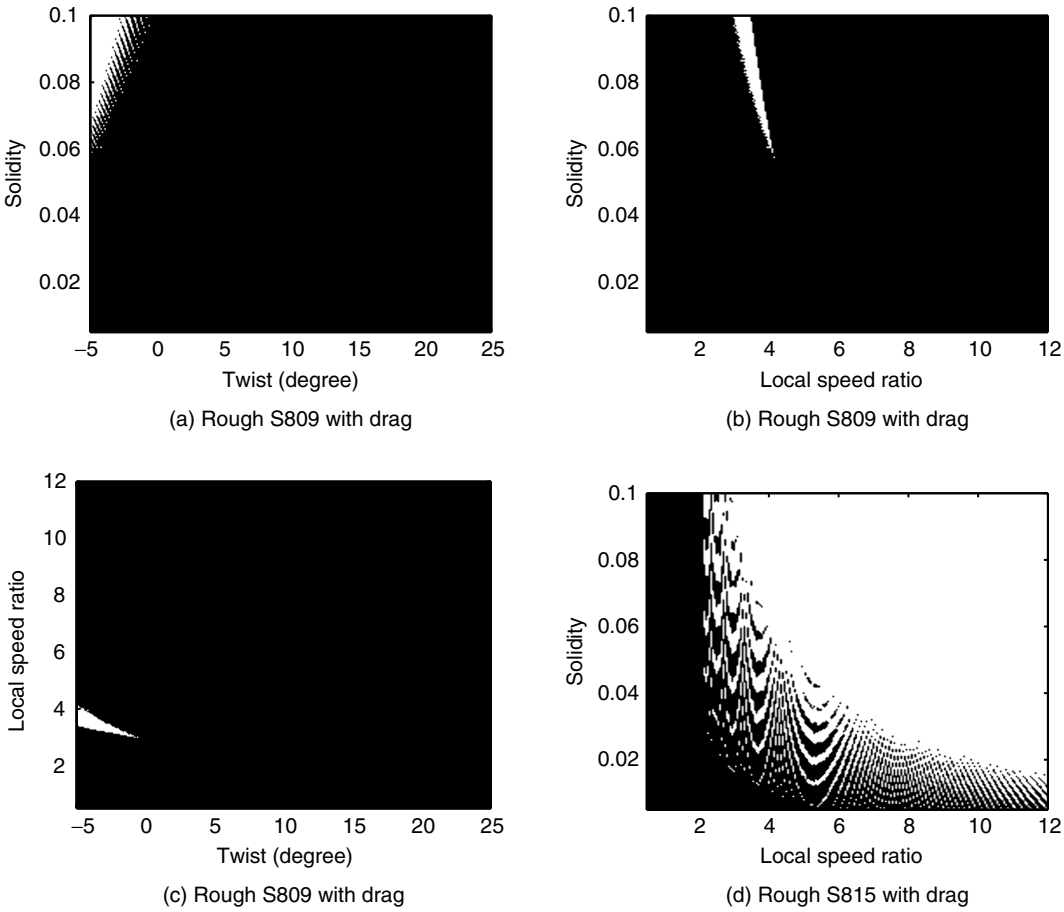

Figure 2: Multiple solution counts over varying range of parameters (1 solution black, 3 solutions white).

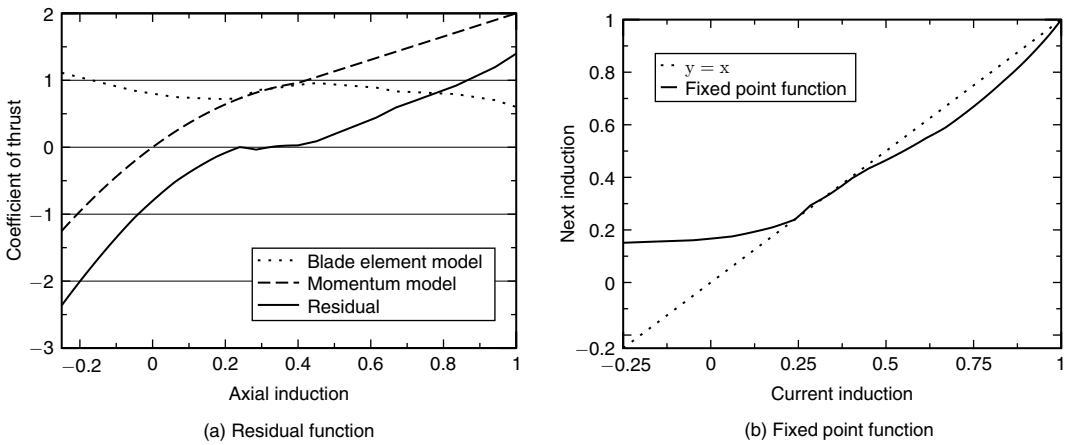

Figure 3: Example of multiple solutions; clean S809 airfoil with drag, $\sigma = 0.0945$, $\lambda = 3.05$ and $\theta = -5^{\circ}$.

Figure 3a shows an example of how the thrust models varied with induction to produce multiple solutions. As expected, when multiple solutions occur, it is because the blade element model follows the momentum model for an interval. The slight variations in the airfoil data for this interval result in multiple solutions. The small slope of the residual function could produce unbounded results close to the solution. Figure 3b shows how the fixed point function would vary for the same point. As expected, the fixed point function lies on the $y = x$ line. Here, the slope is close to unity, consequently the solver would exhibit either slow convergence, or divergence.

Neglecting drag in the calculations had little effect on the number of solutions found. Including drag merely altered the region in the design space where multiple solutions could be found. Inspection of these regions showed similar trends to those shown in figure 3. Accordingly, the effect of drag has a minor role in the existence of multiple solutions.

Overall, the blade element equation (2) is decreasing with increasing drag and lift, thus multiple solutions only occur when there is a decreasing lift coefficient from stall. The validity of the airfoil data here is in question. First, stall is known to give an unsteady force response. Second the nature of stall can vary widely due to turbulence and various other conditions. Finally, for wind turbines in particular, the rotational effects are known to delay stall. Thus these regions of multiple solutions coincide with the regions of greatest uncertainty in the actual physics of the aerodynamic models.

Multiple solutions occur when the blade forces vary with induction, similar to how induction (from the wake structure) varies with forces. In other words, the magnitude and slopes are similar, for both the blade element model and the momentum model. Regardless of the uncertainty in the modeling, these situations could occur in reality. Under these circumstance, the induction is weakly dependent on the blade state and the induction would be more strongly effected by local flow conditions. For example, with all other things being constant, after a gust, the flow would settle into a low induction state, while after a lull, a high induction state. Similarly, variation in the stall forces would also cause changes in the induction state. This weak dependence could be a source of error and uncertainty in modeling turbines when the blades are stalling. Along the interval of multiple solutions, the range of induction is between 0.2 and 0.4, with a variation of lift coefficient between 0.7 and 1.0. This causes significant variations in the blade forces. Given the importance of using stall to regulate some wind turbines and in predicting loads during the turbulent conditions when stall is entered, this could be an important insight for the design of wind turbines.

3.3. Quantifying the Stability of the Numerical Methods

A Newton-Raphson iteration scheme will produce unbounded solutions when the slope approaches 0. The fraction of points that had a residual slope magnitude less than 0.02 was used as a measure of instability. Similarly, when the magnitude of the fixed point function slope is unity or greater, the method will diverge. The percentage of points that exhibited this behaviour was used as a measure of instability for the fixed point iteration scheme. Selected results are tabulated in table 1. Note that the stability measures of each method are not directly comparable, as the nature of the instability is different.

To quantify the various effects present, the average stability of the appropriate set is given in table 2. From this data it is clear that the Newton-Raphson iteration stability is sensitive to grit roughness. This is expected, as a roughened leading edge leads to a more gradual stall, confirming the analytical conclusion that this is beneficial to the stability of Newton-Raphson methods. Comparing the effect of including drag in the calculations shows that it has a minor role in stabilizing the calculations. Overall, the stability of the fixed point function has weak dependence on airfoil properties.

3.3.1. Newton-Raphson iteration

The location within the design space where instability occurred is shown in figure 4. The figure shows contour plots for the Newton-Raphson stability measure. At each point within the contour plot, two design variables are fixed; the plotted value is the average stability for all points of the remaining free design variable. Drag was included in the calculations for all these results. Figure 4b shows that instability occurs in a small region defined by both the local speed ratio and solidity. This confirms the importance of these two parameters, as discussed in section 2.1. The remaining figures show that high twist is also associated with instability. Here, term A of equation (10) is starting to contribute to instability.

The results given in figures 4a through 4c are an example of relatively low stability. When the S813 profile has leading edge roughness, the stability improves significantly. The stability region of the roughened S813 profile with respect to local speed ratio and solidity is given in figure 4d. Here, the location of the instability is less broad, and shifted towards increased local speed ratio and solidity.

Table 1: Stability results for selected profiles

	Rough	Ignoring Drag	Mean Newton-Raphson Instability	Mean Fixed Point Instability
S825	Yes	No	14×10^{-6}	0.18
S809	Yes	No	50×10^{-6}	0.21
S813	Yes	No	329×10^{-6}	0.21
S815	Yes	No	414×10^{-6}	0.18
S809	No	Yes	472×10^{-6}	0.22
S813	No	No	840×10^{-6}	0.20
S825	No	Yes	858×10^{-6}	0.18

Table 2: Stability of selected data sets

Data Set	Mean Newton-Raphson Instability	Mean Fixed Point Instability
Clean Leading Edge	553×10^{-6}	0.20
Rough Leading Edge	270×10^{-6}	0.19
Using Drag	400×10^{-6}	0.20
Ignoring Drag	423×10^{-6}	0.20

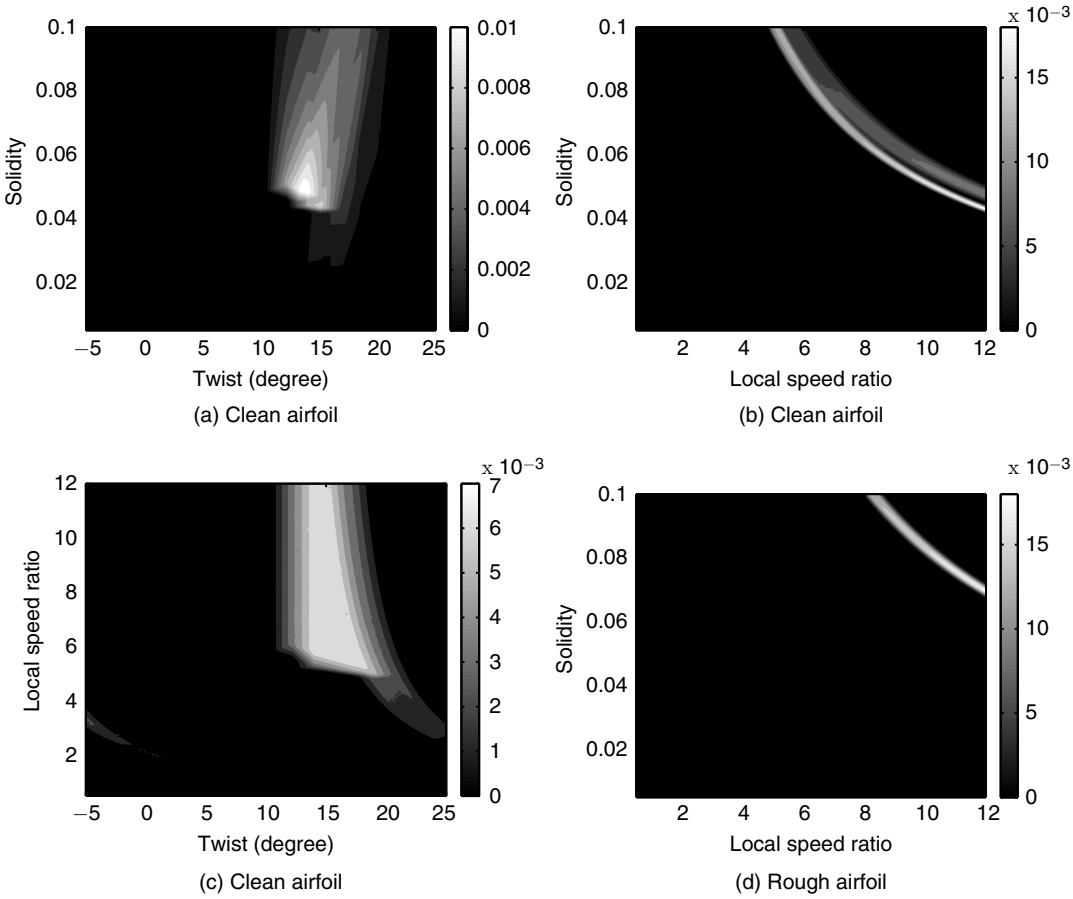

Figure 4: Mean stability measure for Newton-Raphson method with S813 airfoil.

3.3.2. Fixed point iteration

The regions within the design space where the instability occurs for the fixed point iteration function is given in figure 5. As before, each sub-figure is a contour plot showing the average stability across the remaining free variable. The plots shown here were generated with rough S813 data, and are typical for the other airfoils.

The results show that the fixed point iteration function has increased stability for small angles of twist and low solidity. The plot shows increased stability for low local speed ratios. When solidity or twist is also low, then increased stability is present at higher local speed ratios. This region of increased stability corresponds well to design parameters expected in well designed turbines. Despite the seemingly poor stability, this shows that a fixed point scheme is still acceptable for most design applications. However, it is common for most optimization algorithms to test areas in the design space far from the optimum. Accordingly, this algorithm may not be suitable for optimization applications.

3.4. The Effect of Airfoil Data on Stability

To understand how airfoil data affected stability, the angle of attack where instability occurred was recorded for every case. Figure 6a shows the frequency of Newton-Raphson instability conditions at various angles of attack for the S813 airfoil. This figure is typical for other profiles. It is clear from these figures that there is a strong correlation to the angle of attack. This confirms that term B is dominant in equation (10). The greater frequency for negative angles of attack show that term A from equation (10) is also contributing to instability.

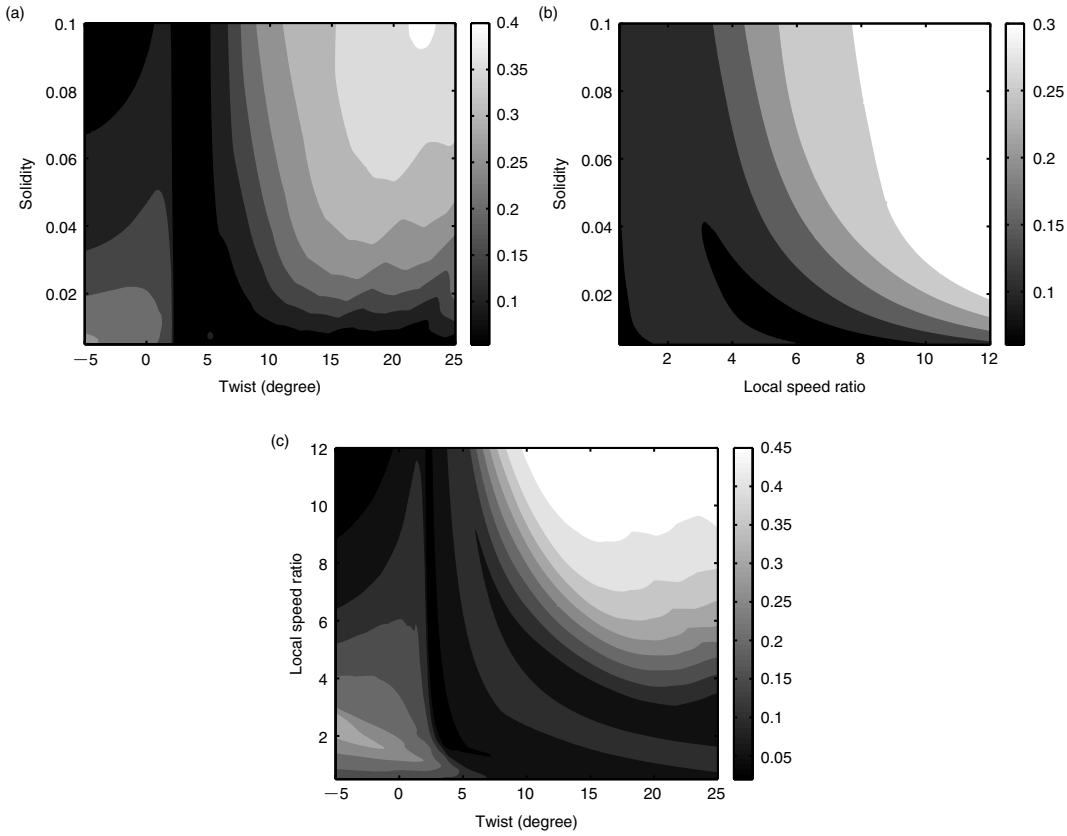

Figure 5: Mean stability measure for fixed point method with the rough S813 airfoil.

The frequency results for the roughened S813 are given in figure 6b. It is clear that instability is confined to specific angles of attack. The difference between clean and rough profiles is the magnitude of the frequency and more importantly the angles where frequency is high. Referring to the lift polar given in figure 6c, it is clear that the high frequency of occurrences correspond with negative lift curve slope.

The data for the fixed point iteration scheme showed that the instability would occur for a wide range of angles of attack. The results for the rough S813 airfoil including drag is given in figure 6d. The instability is strongest for negative angles of attack. This would correspond with the instability region of large twist and high local speed ratio in figure 5c. It is important to note that the region of fixed point instability could not be correlated to airfoil polar data.

3.5. Stability Differences Between Methods

It was demonstrated in section 2.1 that for a Newton-Raphson scheme the stability had a minor dependence on the momentum equation. Provided that this equation is monotonic, the same stability qualities will exist. Any momentum model that is not monotonic with respect to induction violates conservation of momentum, hence it safe to assume that these stability characteristics are universal.

When applying a fixed point iteration scheme, several algebraic manipulations are applied to both the blade element model and the momentum model. A different fixed point function will be developed for each momentum model and choice of analytic manipulation. This fixed point function will then have its own unique stability characteristics. Thus, for the fixed point iteration scheme, it is difficult to draw any conclusions that apply universally.

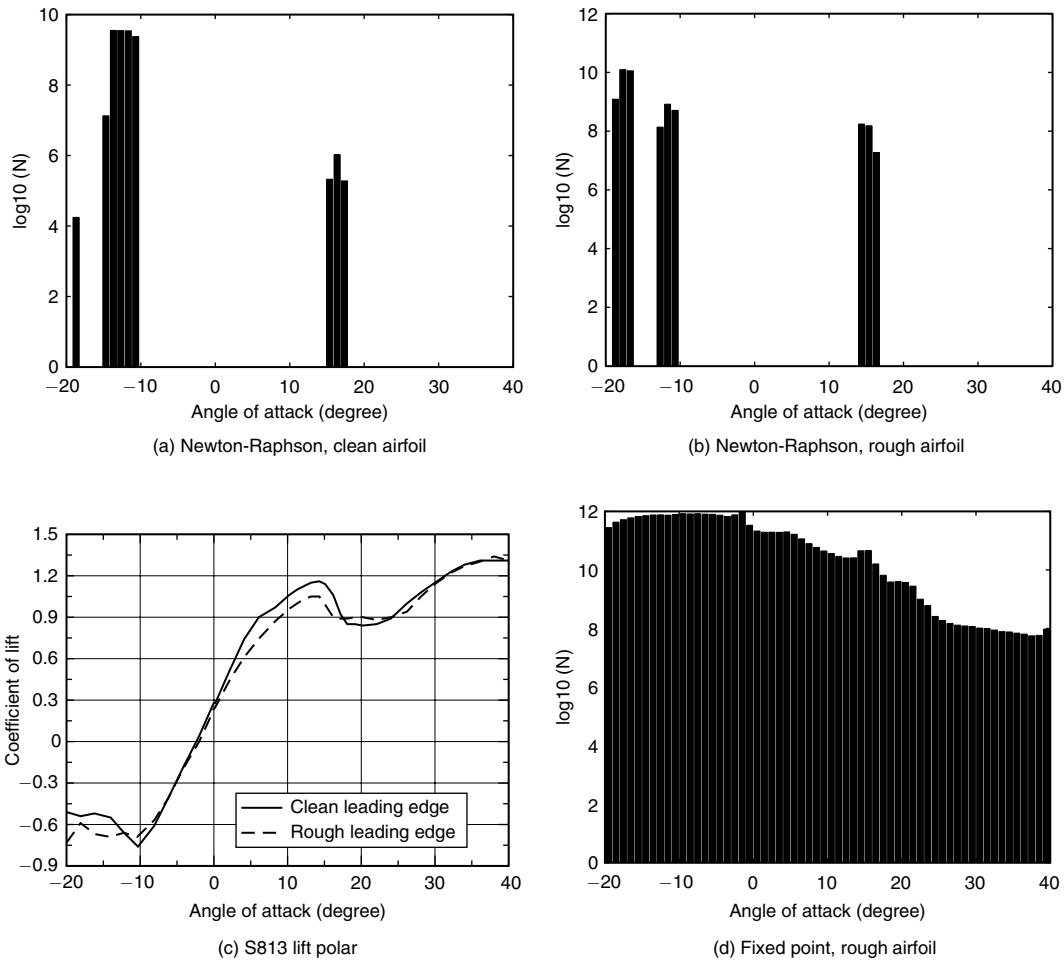

Figure 6: The frequency of instability for the S813 airfoil.

The results here show that the Newton-Raphson iteration scheme is more stable for solving BEM equations than the more widely used fixed point iteration scheme. Yet, these results neglect the nature of the instability. The behavior at the instability has similar importance in selecting the appropriate numerical scheme.

When a Newton-Raphson scheme falls into an unstable region, an unbounded result is produced. This demands techniques for handling these exceptions. A common practice is to limit the maximum change in subsequent solutions. To prevent oscillations in the predicted solution, relaxation could be applied. The detriment here is the difficulty in creating an effective technique for handling these exceptions.

Alternatively, when a fixed point scheme is in an unstable region, it is unlikely to give an unbounded prediction. Instead the scheme will bounce around a collection of reasonable values. Under these circumstances, the common practice is to lag the solution after a given number of iterations. The detriment here is that many iterations must pass for these lagging methods to be activated. For a more unstable fixed point function, the method would be much slower.

In both methods, the algorithm must be able to detect when the method is failing, and have techniques to handle these situations. The results here show that the stability of the Newton-Raphson scheme is tightly tied to the airfoil profile performance data, and is in a well defined

region within the design space. This gives the algorithm many other possibilities to detect unstable regions for the Newton-Raphson scheme. Section 2.2 showed the difficulty in identifying the stability characteristics for a fixed point iteration scheme. For the fixed point function here, the user is forced to iterate a set number of times to detect whether the solution needs lagging. Thus, odd designs will significantly slow this method.

4. CONCLUSIONS

Regardless of the numerical method, the BEM equations can have multiple solutions for a given set of design parameters. These multiple solutions occur over a wide range of induction when the airfoil is stalled. This adds further uncertainty to results obtained in stalled flow. When this occurs, there is evidence that the wake state will be weakly dependent on the blade conditions. This issue is not an artifact of the BEM equations, rather it is likely a reflection of reality. Accordingly, this has implications for other simulation methods and design. If in fact it does exist, then accurate modeling of this condition would require methods more advanced than the current BEM theory.

The analytical investigation into the stability of the Newton-Raphson method showed that the stability is defined almost exclusively by the airfoil characteristics. Furthermore, the particular form of the momentum equation has little significance to the stability characteristics. The numerical calculations confirmed that a Newton-Raphson scheme will give unbounded solutions when there is a negative slope in the c_l vs. α curve, within a small region of the design space defined by the twist and local speed ratio. Given appropriate methods to handle instabilities, the well defined stability criterion is a desirable quality.

The study here investigated the stability of one particular fixed point function. For every version of the BEM equations, there is a unique fixed point function, with its own stability characteristics. Accordingly, it is difficult to draw conclusions that universally apply to all fixed point schemes. For the fixed point function considered in this paper, the numerical instability is present over a wide range of the design space and attack angles, however the method has increased stability in the design space common to well designed turbines. Furthermore, the fixed point iteration does not produce the unbounded solutions common in a Newton-Raphson scheme. The user can use the number of iterations to trigger methods to handle these regions of instability.

The generality and predictable stability of the Newton-Raphson scheme is well suited for research applications where multiple momentum equations will be explored and tested. However, the relatively safe behavior of the fixed point scheme is desirable in a design application. Nevertheless, applying the fixed point scheme may not be practical for more advanced BEM equations. Thus, care must be taken in selecting an appropriate fixed point scheme.

REFERENCES

1. R. Lanzafame and M. Messina. Design and performance of a double-pitch wind turbine with non-twisted blades. *Renewable Energy,* 34:1413–1420, 2009.
2. Zhaohui Du and Michael S. Selig. A 3-D Stall-Delay Model for Horizontal Axis Wind Turbine Performance Prediction. In *AIAA 36th Aerospace Sciences Meeting and Exhibit,* 1998.
3. James L. Tangler and Michael S. Selig. An Evaluation of an Empirical Model for Stall Delay due to Rotation for HAWTs. In *WINDPOWER '97 Conference Austin, Texas, June 15–18, 1997,* 1997.

4. Wen Zhong Shen, Robert Mikkelsen, and Jens Norkaer Sorensen. Tip Loss Corrections for Wind Turbine Computations. *Wind Energy,* 8:457–475, 2005.

5. K. Chaney and A. J. Eggers Jr. Expanding Wake Induction Effect on Thrust Distribution on a Rotor Disc. *Wind Energy,* 5:213–226, 2002.

6. Helge Aa. Madsen, Christian Bak, Mads Dossing, Robert Mikkelsen, and Stig Oye. Validation and modification of the Blade Element Momentum theory based on comparisons with actuator disc simulations. *Wind Energy,* 13:373–389, August 2009.

7. Wouter Haans, Tonio Sant, and Gijs Van Kuik Gerard van Bussel. Stall in Yawed Flow Conditions: A Correlation of Blade Element Momentum Predictions With Experiments. *Journal of Solar Energy Engineering,* 128:472–480, 2006.

8. Curran Crawford. Re-examining the Precepts of the Blade Element Momentum Theory for Coning Rotors. *Wind Energy,* 9:457–478, 2006.

9. D. J. Sharpe. A General Momentum Theory Applied to an Energy-extracting Actuator Disc. *Wind Energy,* 7:177–188, 2004.

10. Tony Burton, David Sharpe, Nick Jenkins, and Ervin Bossanyi. *Wind Energy Handbook.* John Wiley and Sons, Chichester, England, 2001.

11. Jaime Martinez, Luca Bernabini, Oliver Probst, and Ciro Rodriguez. An Improved BEM Model for the Power Curve Prediction of Stall-regulated Wind Turbines. *Wind Energy,* 8:385–402, 2004.

12. Wang Xudong, Wen Zhong Shen, Wei Jun Zhu, Jens Norkaer Sorensen, and Chen Jin. Shape Optimization of Wind Turbine Blades. *Wind Engineering,* 12:781–803, 2009.

13. P. Fuglsang and H. A. Madsen. Optimization method for wind turbine rotors. *Journal of Wind Engineering and Industrial Aerodynamics,* 80:191–206, 1999.

14. M. J. Clifton-Smith and D. H. Wood. Further dual purpose evolutionary optimization of small wind turbine blades. *Journal of Physics: Conference Series,* 75, 2007.

15. M. J. Clifton-Smith. Wind Turbine Blade Optimization with Tip Loss Corrections. *Wind Engineering,* 33:477–496, 2009.

16. Ernesto Benini and Andrea Toffolo. Optimal Design of Horizontal-Axis Wind Turbines Using Blade-Element Theory and Evolutionary Computation. *Journal of Solar Energy Engineering,* 124:357–363, 2002.

17. Curran A. Crawford and Luke Stack. Optimal rotors for distributed wind turbines. In *28th ASME Wind Energy Symposium/47th AIAA Aerospace Sciences Meeting and Exhibit,* Orlando, FL, January 5–8 2009.

18. Curran Crawford and Jim Platts. Updating and Optimization of a Coning Rotor Concept. *Journal of Solar Energy Engineering,* 130, August 2008.

19. R. Lanzafame and M. Messina. Fluid dynamics wind turbine design: Critical analysis, optimization and application of BEM theory. *Renewable Energy,* 32:2291–2305, 2007.

20. Sren Hjort, Kristian Dixon, Michael Gineste, and Anders S. Olsen. Fast Prototype Blade Design. *Wind Engineering,* 33:321–334, 2009.

21. Curran Crawford. *Advanced Engineering Models for Wind Turbines with Application to the Design of a Coning Rotor Concept.* PhD thesis, Trinity College, Department of Engineering, University of Cambridge, October 2006.

22. J. F. Manwell, J. G. McGowan, and A. L. Rogers. *Wind Energy Explained, Theory, Design and Application.* John Wiley and Sons, Chichester, England, 2002.

23. R. Reuss Ramsay, M. J. Hoffmann, and G. M. Gregorek. Effects of Grit Roughness and Pitch Oscillations on the S801 Airfoil. Technical report, National Renewable Energy Laboratories, 1617 Cole Boulevard, Golden, Colorado, United States of America, 1996. NREL/TP-442-7818.

24. R. Reuss Ramsay, M. J. Hoffmann, and G. M. Gregorek. Effects of Grit Roughness and Pitch Oscillations on the S809 Airfoil. Technical report, National Renewable Energy Laboratories, 1617 Cole Boulevard, Golden, Colorado, United States of America, 1995. NREL/TP-442-7817.

25. R. Reuss Ramsay, M. J. Hoffmann, and G. M. Gregorek. Effects of Grit Roughness and Pitch Oscillations on the S810 Airfoil. Technical report, National Renewable Energy Laboratories, 1617 Cole Boulevard, Golden, Colorado, United States of America, 1996. NREL/TP-442-7816.

26. R. Reuss Ramsay and G. M. Gregorek. Effects of Grit Roughness and Pitch Oscillations on the S812 Airfoil. Technical report, National Renewable Energy Laboratories, 1617 Cole Boulevard, Golden, Colorado, United States of America, 1998. NREL/TP-442-8167.

27. R. Reuss Ramsay and G. M. Gregorek. Effects of Grit Roughness and Pitch Oscillations on the S813 Airfoil. Technical report, National Renewable Energy Laboratories, 1617 Cole Boulevard, Golden, Colorado, United States of America, 1996. NREL/TP-442-8168.

28. J. M. Janiszewska, R. Reuss Ramsay, M. J. Hoffman, and G. M. Gregorek. Effects of Grit Roughness and Pitch Oscillations on the S814 Airfoil. Technical report, National Renewable Energy Laboratories, 1617 Cole Boulevard, Golden, Colorado, United States of America, 1996. NREL/TP-442-8161.

29. R. Reuss Ramsay, M. J. Hoffmann, and G. M. Gregorek. Effects of Grit Roughness and Pitch Oscillations on the S815 Airfoil. Technical report, National Renewable Energy Laboratories, 1617 Cole Boulevard, Golden, Colorado, United States of America, 1996. NREL/TP-442-7820.

30. R. Reuss Ramsay, J. M. Janiszewska, and G. M. Gregorek. Effects of Grit Roughness and Pitch Oscillations on the S825 Airfoil. Technical report, National Renewable Energy Laboratories, 1617 Cole Boulevard, Golden, Colorado, United States of America, 1998.

31. James Tangler and J. David Kocurek. Wind Turbine Post-Stall Airfoil Performance Characteristics Guidelines for Blade-Element Momentum Methods. Technical report, National Renewable Energy Laboratories, 1617 Cole Boulevard, Golden, Colorado, United States of America, October 2004.